

Face-gear drive: Meshing efficiency assessment

Journal Article**Author(s):**

Zschippang, Andreas H.; Weikert, Sascha; Wegener, Konrad

Publication date:

2022-05

Permanent link:

<https://doi.org/https://doi.org/10.3929/ethz-b-000532583>

Rights / license:

[Creative Commons Attribution 4.0 International](#)

Originally published in:

Mechanism and Machine Theory 171, <https://doi.org/10.1016/j.mechmachtheory.2022.104765>



Research paper

Face-gear drive: Meshing efficiency assessment

H. Andreas Zschippang^{a,*}, Sascha Weikert^a, Konrad Wegener^b^a Inspire AG, Zürich, Switzerland^b Institute of Machine Tools and Manufacturing, ETH Zürich, Switzerland

ARTICLE INFO

Keywords:

Face-gear
 Meshing efficiency
 Coefficient of friction
 Elastohydrodynamic lubrication
 Transmission test bench
 Tooth contact analysis

ABSTRACT

The estimation of the losses due to friction of meshing tooth flanks is an important point in the design of gear drives. In addition to other design factors, the efficiency of a gear stage is an important criterion for selecting the type of gear and the number of gear stages in order to achieve a desired gear ratio. This manuscript deals with various approaches with which the friction losses that result from the meshing flanks of a face-gear stage can be estimated. In addition, the influence of the directions of sliding and rolling speed is investigated, which is particularly important for gear stages with axle offset, since the two velocities are not collinear. The calculation method is validated for low speeds by means of experiments on a transmission test bench.

1. Introduction

An important point for the design of gearboxes is the estimation of the efficiency or the loss due to friction. First studies on this subject date from the 19th century, e.g. the publication of Reuleaux [1]. But above all the numerous publications on this topic, as reviewed for example by Martin [2] and Yada [3], underline its importance.

The total power loss in a gear transmission is the sum of the load-dependent mechanical power losses and the speed-dependent power losses. The load-dependent mechanical power losses are produced by friction due to relative sliding and rolling between the lubricated mating contact surfaces of the gear flanks and the bearings. The speed-dependent power losses are produced by churning and windage losses. According to Mba and Heingartner [4], windage losses result from increased air resistance due to the oil mist in the gearbox housing and the turbulence caused by rotating parts. Churning losses arise as a result of the movements and circulation of the lubricant within the housing. In gears, inclusions of the lubricant between the teeth are also included. Therefore, the speed-dependent power losses includes drag losses of all rotating elements, all viscous losses, e.g. in the bearings and seals, and losses due to adhesion of the lubricant at the mating gear surfaces.

One way to determine the load-dependent mechanical power loss when the tooth flanks engage (gear mesh power loss), so the power loss purely produced by friction of the mating gear flanks, is to carry out experimental tests. Petry-Johnson et al. [5] show that the mechanical gear mesh power loss can be estimated by performing tests under loaded and unloaded conditions, which are used to distinguish between mechanical and oil churning losses. The bearing losses that are part of the measurements are estimated separately and deducted from the measurement results. Furthermore, experimental investigations on spur gears were performed by Yada [6], Naruse et al. [7,8], as well as Mitzutani and Ishikawa [9]. Talbot et al. [10] made experimental studies on the efficiency of planetary gears and Vaidyanathan [11] made experiments on helical gears.

The real interest is, of course, the determination of a mathematical model that predicts the loss due to friction. The mechanical gear mesh power loss model requires a method for calculating the friction coefficient for the mating gear contact surfaces. Denny [12], Pedrero et al. [13], Pleguezuelos et al. [14] as well as Michlin and Myunster [15] assume a constant friction coefficient along the entire flank contact surface for involute gears.

* Corresponding author.

E-mail address: zschippang@inspire.ethz.ch (H. Andreas Zschippang).

Nomenclature

Specific Symbols

$\Delta\gamma, \Delta E, \Delta a$	Alignment errors
ΔP	Meshing power loss
$\Delta P^{(m)}$	Meshing power loss in section m
ΔP_i	Total power loss
$\Delta P_{bearing_i}$ ($i = 1, 2$)	Bearing power loss
ΔP_{oil_i} ($i = 1, 2$)	Oil churning power loss
ΔP_{seal_i} ($i = 1, 2$)	Seal power loss
$\epsilon_i^{(v)}$ ($i = 1, 2$)	Angle between the base vector \underline{v} of the contact ellipse and the first principal direction \underline{t}_{jI}
ϵ_γ	Total contact ratio
η	Average/overall meshing efficiency containing sliding and rolling frictional losses
η'	Instantaneous meshing efficiency
γ	Shaft angle
κ, κ_i ($i = 1, 2$)	Curvature
$\kappa_{iI}, \kappa_{iII}$ ($i = 1, 2$)	Principal curvature
μ_f	Coefficient of friction
ν_d	Dynamic viscosity at oil inlet under ambient pressure
ν_k	Kinematic viscosity
ν_i ($i = 1, 2$)	Poisson's ratio
ω, ω_i ($i = 1, 2$)	Rotational speed
ω_{in}	Rotational speed of input shaft
ϕ_i, ϕ_{in} ($i = 1, 2$)	Angle of rotation
σ	Angle between vectors of first principal directions in contact point of two mating bodies
Σ, Σ_i ($i = 1, 2$)	Flank surface
$\underline{M}_{f'i}$ ($i = 1, 2$)	Matrix of coordinate transformation from coordinate system S_i to fixed coordinate system $S_{f'}$
$\underline{L}_{f'1}$	Upper-left 3×3 sub-matrix of $\underline{M}_{f'1}$
\underline{q}	Evaluation direction
$\underline{r}, \underline{r}_i$ ($i = 1, 2$)	Position vector of flank surface
$\underline{r}^{(f')}$	Point on the major semi-axis of the contact ellipse
$\underline{r}_c^{(f')}$	Contact point
$\underline{t}_c^{(f')}$	Tangential vector of contact point
$\underline{v}, \underline{s}$	Base vectors of contact ellipse
\underline{v}_i ($i = 1, 2$)	Velocity of a surface point
$\underline{v}_i^{(f')}$ ($i = 1, 2$)	Orthogonal projection of the velocity
ζ	Angle between direction vector \underline{q} and the main direction vector \underline{s} of the contact ellipse
a, b	Half axes of contact ellipse
C_m	Dimensionless drag torque
E	Axle offset
E'	Equivalent stiffness
E_i ($i = 1, 2$)	Young's modulus
F_r	Radial pretension force
Fr	Froude number
h_d	Gear immersion depth
N	Number of angular positions
N_i ($i = 1, 2$)	Number of teeth
n_i ($i = 1, 2$)	Rotational speed
P_{in}	Input power
p_{max}	Maximum contact pressure

Many publications which contain experimental data [7,16–20] indicate that the assumption of a constant friction coefficient for mating gear contact surfaces is only a rough approximation. The resulting instantaneous friction coefficient depends on the sliding velocity, the rolling velocity, the lubricant viscosity, the load, the radii of curvature and the surface roughness. Misharin [16],

P_{out}	Output power
R	Radius, Equivalent radius of contact surfaces
R_i ($i = 1, 2$)	Radius of contact surface, radius of replacement cylinder
R_q	Equivalent radius in evaluation direction
R_{shaft}	Shaft radius
Ra	Center line average surface roughness
Re	Reynolds number
Re_c	Critical Reynolds number
S, S_{CLA}, S_{RMS}	Surface roughness, CLA...center line average, RMS...root mean square
S_i ($i = 1, 2, m, p, f'$)	Coordinate system
S_m	Submerged surface area
S_r	Slide-to-roll ratio
T, T_i ($i = 1, 2$)	Torque
T_{ch}	Oil churning torque
T_{in}	Input torque
T_{oil}	Oil inlet temperature
T_{seal}	Frictional torque in seal
v_e	Lubricant entry speed
v_i ($i = 1, 2$)	Surface speed
v_r	Rolling speed
v_s	Sliding speed
$v_{r,q}$	Rolling speed in evaluation direction
$v_{s,max}$	Maximum sliding speed
$v_{s,q}$	Sliding speed in evaluation direction
v_{ii} ($i = 1, 2$)	Peripheral speed of a surface point
w	Tooth width
W'	Unit load
x_i ($i = 1, 2, m, p, f'$)	x-axis of the coordinate system i
y_i ($i = 1, 2, m, p, f'$)	y-axis of the coordinate system i
z_i ($i = 1, 2, m, p, f'$)	z-axis of the coordinate system i

Subscripts

i	1... pinion, 2... face-gear
n	Angular position, $n = 1...N$

Benedict and Kelley [17] as well as Drozdov and Gavrikov [18] simulated a gear contact on a roller test machine and combined the results in formulae which represent the data. The influence of the surface roughness is not taken into account. O'Donoghue and Cameron [19] and Ku et al. [20] also examined the friction of rolling sliding contacts using a roller testing machine, but also considering the surface roughness. Tests to determine the frictional loss of spur gears using a gear testing machine were conducted by Naruse et al. [7]. Further experimental formulae are those of Kelley and Lemanski [21], who also take the surface roughness into account, and those of Johnson and Tevaarwerk [22].

As an enhancement compared to the assumption of a constant friction coefficient along the entire flank contact surface, Anderson and Loewenthal [23–27] applied the experimental formula for the friction coefficient published by Benedict and Kelley [17] to predict the power loss of spur gears. Heingartner and Mba [28] used this approach for helical gears. Dong et al. [29] use the modified empirical formula of Benedict and Kelley to predict the meshing efficiency of a spur face-gear. Xu [30], Ratanasumawong et al. [31] and Yenti et al. [32] compare the friction losses calculated using the various empirical equations with experimental results for parallel-axis gear pairs.

Diab et al. [33] emphasize that the empirical formulae of Benedict and Kelley [17] and Kelley and Lemanski [21] were obtained from specimens with a surface finish parallel to the rolling direction. Since the surface finish of a gear is perpendicular, both formulae tend to overestimate the friction coefficient. In addition, the experiments were conducted for high slide-to-roll ratios; at low slide-to-roll ratios, such as those that occur in contact near the pitch circle, the friction coefficient is also overestimated. Diab et al. [33] therefore developed a friction model that covers a reasonable range of slide-to-roll ratios and validated the model through experiments carried out on a transmission test bench.

In order to increase the accuracy, elastohydrodynamic lubrication (EHL) friction models were developed. For spur gears, Dowson and Higginson [34,35], Martin [36] and Simon [37] use EHL formulae to determine the distribution of surface shear stress, taking

smooth tooth flanks into account, while the latter focuses on point contact on crowned gears. Wu and Cheng [38], Xu et al. [39], Li et al. [40] and Li and Kahraman [41] improved the EHL models to take the surface roughness into account. Simon [42,43] developed a model to calculate the efficiency of hypoid gears, also considering mixed elastohydrodynamic lubrication. The models of Li et al. [40,41] use boundary EHL formulations that are relevant for low load or low speed gear transmissions because of the metal to metal contact.

In the field of face-gear drives, Saribay [44] uses the generalized film thickness formula of Dowson [45] to estimate the friction loss of conjugate meshing face-gear pairs for elastohydrodynamic lubrication. Dong et al. [29] apply empirical friction coefficient formulae to calculate the friction loss of a face-gear drive with a spur pinion.

The approach of using a physics-based EHL model is also used by Xu and Kahraman [30,46] for hypoid gear drives; however, there is no application and validation of this approach for face-gear drives. Furthermore, the influence of very strongly deviating directions of the roll and sliding velocity, as is to be expected, for example, in face-gears with an axle offset, has not been the subject of previous research.

In this manuscript, a method for calculating the meshing efficiency by means of a physically-based model for calculating friction coefficients is described. The results are experimentally tested on a transmission test bench. It is shown that the directions of sliding and rolling speed must be taken into account.

2. General approach of determination of meshing efficiency

The approach to determine the meshing efficiency of the transmission is based on the method of Xu [30]. The whole procedure is as follows:

- For a given design of the gear stage, the operating conditions, like angular velocity of the pinion ω_1 , the applied torque T and alignment errors are defined.
- A loaded tooth contact analysis (LTCA) is performed for a number of N angular positions of the pinion ϕ_{1_n} . The angle between the different angular positions $\Delta\phi$ depends on the number of teeth of the pinion N_1 and is calculated by

$$\Delta\phi = \frac{2\pi}{N_1 N} \quad (1)$$

- The contact ellipse is determined for each tooth flank that is in mesh at the pinion rotation angle ϕ_{1_n} . The determined contact ellipses are divided into M sections.
- For each section the equivalent unit load $W'^{(m)}$, the working surface curvatures and the surface speeds $v_1^{(m)}$ and $v_2^{(m)}$ are determined. The coefficient of friction $\mu_f^{(m)}$ is determined using these parameters. Additional parameters such as surface roughness S and lubricant parameters, e.g. the viscosity ν_d , are taken into account. With the coefficient of friction $\mu_f^{(m)}$ determined in this way, the power loss $\Delta P^{(m)}(\phi_{1_n})$ in each section can be calculated.
- The total power loss $\Delta P(\phi_{1_n})$ is therefore the sum of all power losses across the sections. With this total power loss, the instantaneous meshing efficiency η' for the current pinion rotation angle ϕ_{1_n} can be calculated:

$$\eta'(\phi_{1_n}) = \frac{P_{out}}{P_{in}} = \frac{P_{in} - \sum_{m=0}^{M-1} \Delta P^{(m)}(\phi_{1_n})}{P_{in}} = 1 - \frac{\sum_{m=0}^{M-1} \Delta P^{(m)}(\phi_{1_n})}{T_{in} \omega_{in}} \quad (2)$$

The input power P_{in} is the product of the input torque T_{in} and the applied angular speed ω_{in} .

- The power loss and the instantaneous meshing efficiency are calculated for all angular positions ϕ_{1_n} of the pinion and based on this, the overall meshing efficiency η is determined.

Fig. 1 shows the method for predicting the meshing efficiency in the form of a flow chart.

3. Determination of the friction coefficient for EHL

Due to a changing curvature over the tooth flanks, variable surface roughness and variable loads, the contact between a pinion and face-gear flank cannot simply be described as a 2D contact problem. A common approach is therefore to discretize the contact zone, in the best case approximately a contact ellipse, in several sub-areas in which the contact is approximately described as the contact between two replacement cylinders. For this type of contact problem, some formulae are already available for determining the coefficient of friction. In this way, the friction loss can be added up over the individual increments, with which the total friction loss on the rolling tooth flanks can be calculated. This section describes different approaches for calculating the coefficient of friction for the contact between two cylinders.

3.1. Essential parameters influencing the friction coefficient

The main parameters influencing the coefficient of friction are the load applied, the velocities of both contact surfaces, the surface curvatures, the Young's moduli and Poisson's ratios of the contact bodies and the prevailing surface roughness.

With regard to the velocities of the contacting surfaces, a distinction is made among three different velocities:

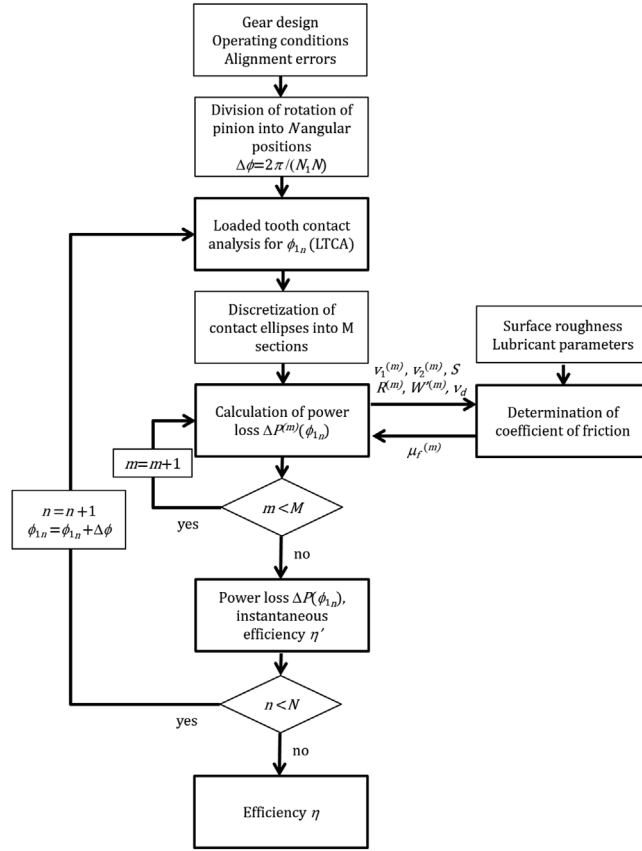


Fig. 1. Flow chart for calculating the meshing efficiency based on Xu [30].

- The sliding speed v_s is the difference between the speeds v_1 and v_2 of the two contact bodies at the contact point or the two replacement cylinders at the contact line, respectively

$$v_s = v_1 - v_2 \tag{3}$$

- The rolling speed v_r is the sum of both speeds v_1 and v_2

$$v_r = v_1 + v_2 \tag{4}$$

- The lubricant entry speed v_e is the average speed of the speeds v_1 and v_2

$$v_e = \frac{v_1 + v_2}{2} = \frac{v_r}{2} \tag{5}$$

The ratio of sliding to rolling is expressed by the dimensionless slide-to-roll ratio

$$S_r = 2 \frac{v_1 - v_2}{v_1 + v_2} = 2 \frac{v_s}{v_r} \tag{6}$$

The surface curvatures are usually taken into account by the radii of the replacement cylinders. The individual radius R_i here is simply the reciprocal of the curvature κ_i

$$R_i = \frac{1}{\kappa_i} \tag{7}$$

The contact between two cylinders can also be converted into an equivalent contact between a cylinder and a plane. According to Popov [47], the radius R of this cylinder is then calculated by

$$R = \frac{R_1 R_2}{R_1 + R_2} = \frac{1}{\kappa_1 + \kappa_2} \tag{8}$$

Fig. 2 shows the contact between two surfaces and its equivalent contact between two cylinders or, derived therefrom, an equivalent contact between cylinder and plane.

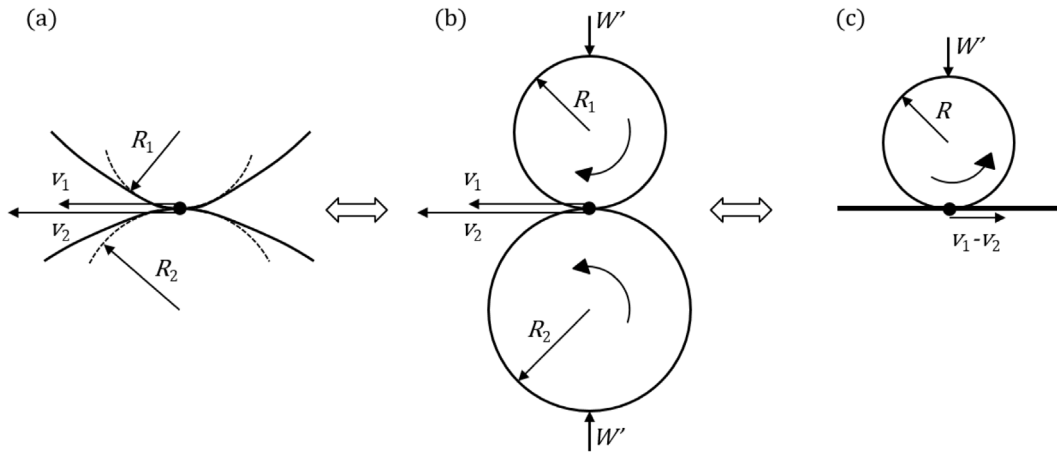


Fig. 2. Contact between two surfaces: (a) surface contact (schematically); (b) equivalent contact cylinder/cylinder; (c) equivalent contact cylinder/plane.

Since the contact surfaces deform with EHL contact, the stiffness of the materials is also important. The relevant parameters are the Young’s moduli E_i and Poisson’s ratios ν_i . The equivalent stiffness E' for both bodies in contact is determined by

$$E' = \frac{2E_1E_2}{E_1(1 - \nu_2^2) + E_2(1 - \nu_1^2)} \tag{9}$$

For the line contact resulting from cylinders, the applied load can be well described by means of the maximum contact pressure p_{max} . More common, however, is the description using the line load W' , i.e. the force applied per unit contact length. Using Hertz’s theory, the relationship between the maximum contact pressure p_{max} and the line load W' for the line contact between two cylinders can be described using the following equation

$$p_{max} = \sqrt{\frac{W'E'}{2\pi R}} \tag{10}$$

If the surface roughness was largely not taken into account at the beginning, it was soon discovered that this also influences the friction in the EHL contact. The typical surface roughness parameter used is S_{RMS} (root mean squared), which is calculated as the root mean square of a surfaces peaks and valleys

$$S_{RMS} = \sqrt{\frac{1}{x_2 - x_1} \int_{x_1}^{x_2} y(x)^2 dx} \tag{11}$$

where $y(x)$ is the profile height function and the term $x_2 - x_1$ describes the evaluation length.

3.2. Friction coefficient formula based on EHL model

In the 1960s in particular, extensive investigations were carried out, primarily using twin-disk test rigs, in order to understand and quantify the losses in the lubricated contact. As a result, numerous empirical formulae have been developed to estimate the coefficient of friction in the lubricated contact. Some have been supplemented or modified over time in order to incorporate further parameters that were not previously taken into account. Nevertheless, it is generally noticeable that some parameters are still neglected in the respective empirical equation. Some examples of such empirical formulae are the formula of Misharin [16], the formula of ISO TC60 [48], the formula of Benedict and Kelley [17], the formula of O’Donoghue and Cameron [19], the formula of Kelley and Lemanski [21], and the formula of Drozdov and Gavrikov [18].

The empirical equations for the coefficient of friction are associated with some disadvantages: The neglect of some parameters, the inaccuracy or faultiness in the case of small slide-to-roll ratios and the partially limited parameter range. For this reason, Xu [30] has developed a correlation for the coefficient of friction that is based on a physical EHL model.

The underlying physical model that Xu [30] relies on is the deterministic EHL model by Cioc et al. [49], which is applicable to line contact. In order to calculate the distribution of the lubricant film pressure and the film thickness over an EHL contact, the following equations are solved simultaneously in this model [49]: The Reynolds equation, the film thickness equation, the viscosity–pressure–temperature relationship, the density–pressure–temperature relationship, the energy balance equation and the load equation.

Since solving the equations of the EHL model is numerically quite complex, such a model is less suitable in practice for the design of gears due to the longer computing times. For this reason, Xu [30] had the idea of generating the solutions using the EHL model with many different data sets, which were sensibly selected for the area of gears, in order to generate a correlation equation

Table 1
Coefficients for EHL based formula by Xu [30].

Coefficient	Value
b_1	-8.916465
b_2	1.03303
b_3	1.036077
b_4	-0.354068
b_5	2.812084
b_6	-0.100601
b_7	0.752755
b_8	-0.390958
b_9	0.620305

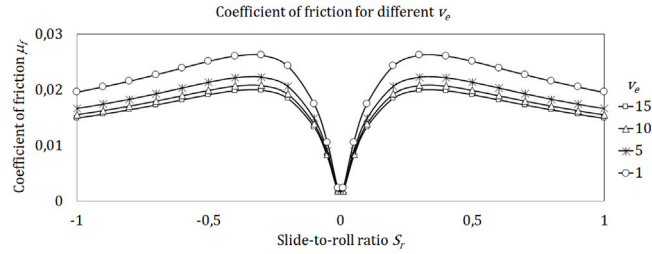


Fig. 3. Calculated coefficient of friction using the physics-based friction coefficient formula according to Xu [30]. $p_{max} = 1.5$ GPa, $R = 5$ mm, $S_{RMS} = 0.07$ μ m.

using mathematical linear regression. A total of around 10,000 EHL analyses were carried out with the widely used 75W90 gear oil as the selected lubricant [30]. The formula obtained using linear regression is as follows

$$\mu_f = e^{f(S_r, p_{max}, v_d, S_{RMS})} p_{max}^{b_2} |S_r|^{b_3} v_e^{b_6} v_d^{b_7} R^{b_8} \tag{12}$$

with $f(S_r, p_{max}, v_d, S_{RMS}) = b_1 + b_4 |S_r| p_{max} \log(v_d) + b_5 e^{-|S_r| p_{max} \log(v_d)} + b_9 e^{S_{RMS}}$

The associated coefficients are listed in Table 1.

Fig. 3 shows the curves of the coefficients of friction versus the slide-to-roll ratio using the physics-based formula according to Xu [30] for selected conditions.

With the friction coefficient formula by Xu [30], the gear meshing efficiency can be determined in the shortest possible time, taking into account all relevant influencing variables.

4. Application of friction models on face-gear drives

The formula of Xu [30] given in Eq. (12) has been applied to various types of gears. Xu et al. [39] applied it to predict the mechanical efficiency of spur gears and Xu and Kahraman [46] applied it also to hypoid gear pairs. The use of face gears has not yet been tested and validated. This section explains the application of the formula of Xu [30] to determine the meshing efficiency of a face-gear stage.

4.1. Relative velocities and equivalent curvature

In a first step, the contact points $r_c^{(f')}$ between pinion and face-gear for different pinion rotation angles ϕ_1 as well as the associated contact ellipses in the fixed coordinate system $S_{f'}$ are determined by means of a loaded tooth contact analysis (LTCA). When calculating the load sharing, the elasticity of the teeth must be taken into account. In this case, a semi-analytical approach is used. Using Hertzian theory of non-adhesive elastic contact [50], the contact ellipses are calculated for a pair of teeth. The pressure distribution is approximated by nodal forces, where the nodal forces are applied to separate FE models of pinion and face-gear. The tooth pair stiffness is determined as a function of torque and pinion rotation angle via the determined displacements. Based on this, the load distribution and the transmission error are calculated. The procedure is explained in detail in [51]. The investigations as described in [51] have shown that the flank contact of a face-gear drive with a spur involute pinion can be calculated well using the Hertzian theory. In order to determine the velocities of both gears along the major semi-axis direction \underline{s} of the contact ellipse, it is assumed that both bodies are flattened onto the contact plane as a result of the Hertzian contact. The very small deviations from this assumption for steel gears are neglected, since the expected Hertzian approach δ of both flanks is generally small. An arbitrary point $r_c^{(f')}$ on the major semi-axis of the contact ellipse in the fixed coordinate system $S_{f'}$ can be calculated by

$$\underline{r}_c^{(f')} = \underline{r}_c^{(f')} + w \frac{\underline{s}}{|\underline{s}|} \tag{13}$$

with $-a < w < +a$

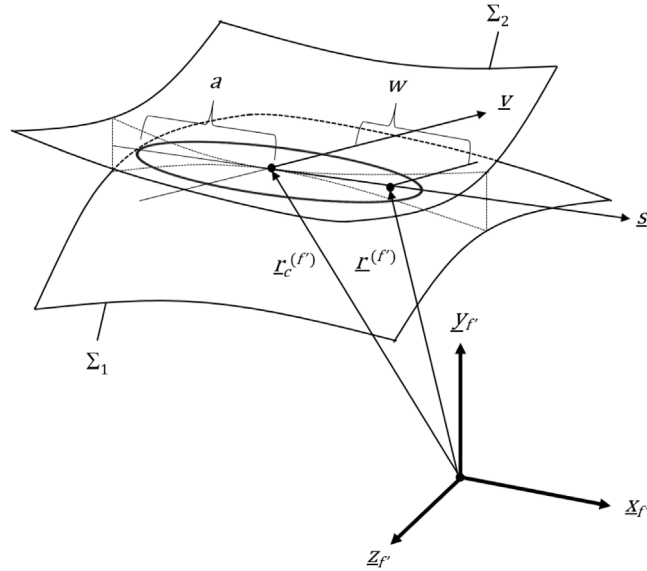


Fig. 4. Surfaces in contact and the corresponding contact ellipse illustrated in the fixed coordinate system S_f .

Fig. 4 shows the contacting surfaces and the contact ellipse.

The corresponding point r_1 represented in the pinion coordinate system S_1 is given by

$$r_1^* = \underline{\underline{M}}_{f'1}^{-1}(\phi_1)r_c^{(f')*}$$

$$\text{with } r_c^{(f')*} = \begin{bmatrix} r_x^{(f')} \\ r_y^{(f')} \\ r_z^{(f')} \\ 1 \end{bmatrix}, r_1^* = \begin{bmatrix} r_{1,x} \\ r_{1,y} \\ r_{1,z} \\ 1 \end{bmatrix} \tag{14}$$

where $\underline{\underline{M}}_{f'1}^{-1}$ is the inverse matrix of $\underline{\underline{M}}_{f'1}$. The transformation matrix $\underline{\underline{M}}_{f'1}$ describes the sequential coordinate transformations to transform a point given in the pinion coordinate system (system rotating with the pinion) to the coordinate system S_f :

- Rotation of pinion around pinion rotation axis z_1 by pinion rotation angle ϕ_1 .
- Rotation of pinion around axis x_m/x_p by shaft angle γ and angular alignment error $\Delta\gamma$.
- Shift of pinion about distance E (axle offset) and alignment error ΔE along direction x_p . Shift of pinion about alignment error Δa along direction y_p .

The set of coordinate transformations is shown in Fig. 5.

The transformation matrix $\underline{\underline{M}}_{f'1}$ is given by

$$\underline{\underline{M}}_{f'1} = \begin{bmatrix} \cos \phi_1 & -\sin \phi_1 & 0 & -E - \Delta E \\ \cos(\gamma - \Delta\gamma) \sin \phi_1 & \cos(\gamma - \Delta\gamma) \cos \phi_1 & -\sin(\gamma - \Delta\gamma) & \Delta a \sin\left(\frac{\pi}{2} - \gamma\right) \\ \sin(\gamma - \Delta\gamma) \sin \phi_1 & \sin(\gamma - \Delta\gamma) \cos \phi_1 & \cos(\gamma - \Delta\gamma) & \Delta a \cos\left(\frac{\pi}{2} - \gamma\right) \\ 0 & 0 & 0 & 1 \end{bmatrix} \tag{15}$$

In Fig. 6, the alignment errors and the shaft angle are shown.

The velocity v_1 of that contact point in the pinion coordinate system is calculated by

$$v_1 = \omega_1 \times r_1 \tag{16}$$

where ω_1 is the vector of rotational speed. Since the pinion is rotating around its z-axis, this vector is defined as

$$\omega_1 = \begin{bmatrix} 0 \\ 0 \\ \omega_1 \end{bmatrix} \tag{17}$$

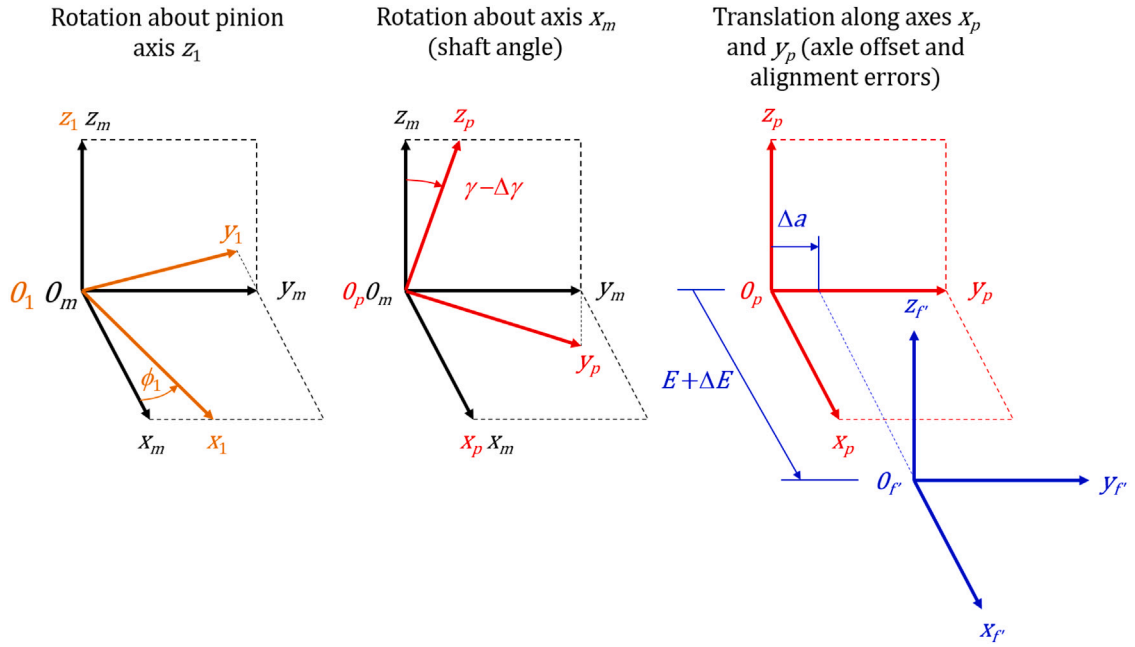


Fig. 5. Coordinate transformations from coordinate system rotating with pinion to coordinate system $S_{f'}$.

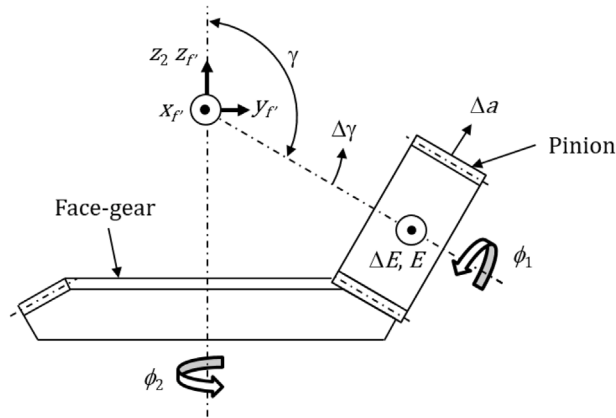


Fig. 6. Definition of alignment errors.

For the pinion velocity $\underline{v}_1^{(f')}$ represented in the fixed coordinate system $S_{f'}$ follows

$$\underline{v}_1^{(f')} = \underline{\underline{L}}_{f'1}(\phi_1)\underline{v}_1 \tag{18}$$

where matrix $\underline{\underline{L}}_{f'1}(\phi_1)$ is the upper-left 3 x 3 sub-matrix of $\underline{\underline{M}}_{f'1}(\phi_1)$.

The velocity of the face-gear is calculated in an analogous manner. The corresponding point \underline{r}_2 of point $\underline{r}^{(f')}$ represented in the face-gear coordinate system S_2 (system rotating with the face-gear) is calculated by

$$\underline{r}_2 = \underline{\underline{M}}_{f'2}^{-1}(\phi_2)\underline{r}^{(f')} \tag{19}$$

where $\underline{\underline{M}}_{f'2}^{-1}$ is the inverse matrix of $\underline{\underline{M}}_{f'2}$. The transformation matrix $\underline{\underline{M}}_{f'2}$ describes a rotation about the face-gear rotation axis z_2 and is represented by

$$\underline{\underline{M}}_{f'2} = \begin{bmatrix} \cos \phi_2 & -\sin \phi_2 & 0 \\ \sin \phi_2 & \cos \phi_2 & 0 \\ 0 & 0 & 1 \end{bmatrix} \tag{20}$$

where the face-gear rotation angle ϕ_2 results from the tooth contact analysis. The velocity \underline{v}_2 of the face-gear point in the face-gear coordinate system is calculated by

$$\underline{v}_2 = \underline{\omega}_2 \times \underline{r}_2 \tag{21}$$

where $\underline{\omega}_2$ is the vector of rotational speed. Since the pinion is rotating around its z-axis, this vector is defined as

$$\underline{\omega}_2 = \begin{bmatrix} 0 \\ 0 \\ \omega_2 \end{bmatrix} \tag{22}$$

For the velocity of the face-gear $\underline{v}_2^{(f')}$ represented in the fixed coordinate system $S_{f'}$ follows

$$\underline{v}_2^{(f')} = \underline{M}_{f'2}(\phi_2)\underline{v}_2 \tag{23}$$

The rotational speed ω_2 of the face-gear can roughly be calculated using the transmission ratio obtained from the ratio of the number of teeth of the pinion N_1 and the face-gear N_2

$$\omega_2 = \frac{N_1}{N_2} \omega_1 \tag{24}$$

However, modifications to the tooth flanks and some alignment errors lead to a variable rotational speed of the face-gear. In this case it makes sense to determine the velocity of rotation ω_2 directly from the velocity of the pinion represented in the fixed coordinate system $S_{f'}$. The tangential component of the velocity of the pinion $\underline{v}_{c1}^{(f')}$ at the contact point $\underline{r}_c^{(f')}$ with respect to the z-axis of the fixed coordinate system $S_{f'}$ thus corresponds to the peripheral velocity v_{i2} of the face gear at this point. The tangential vector $\underline{t}_c^{(f')}$ of point $\underline{r}_c^{(f')}$ is

$$\underline{t}_c^{(f')} = \begin{bmatrix} r_{c_y}^{(f')} \\ -r_{c_x}^{(f')} \\ 0 \end{bmatrix} \tag{25}$$

The peripheral speed v_{i2} results from the length of the orthographic projection of the pinion velocity $\underline{v}_{c1}^{(f')}$ onto the tangential vector $\underline{t}_c^{(f')}$

$$v_{i2} = \underline{v}_{c1}^{(f')} \cdot \frac{\underline{t}_c^{(f')}}{|\underline{t}_c^{(f')}|} \tag{26}$$

For the rotational speed ω_2 of the face-gear follows

$$\omega_2 = \frac{v_{i2}}{\sqrt{r_{c_x}^{(f')^2} + r_{c_y}^{(f')^2}}} \tag{27}$$

The direction vector \underline{q} is introduced to determine the sliding speed v_{s_q} and the rolling speed v_{r_q} for any point $\underline{r}^{(f')}$ on the major axis of the contact ellipse in its direction. The direction vector \underline{q} lies tangentially on the contact ellipse and is rotated by an angle ζ with respect to the main direction vector \underline{s} of the contact ellipse. The two velocities $\underline{v}_1^{(f')}$ and $\underline{v}_2^{(f')}$ are orthographically projected onto the direction vector \underline{q} in order to calculate the sliding and rolling speeds v_{s_q} and v_{r_q} . In Fig. 7, the contact ellipse and the required vectors are shown.

The orthographic projections of the velocities $\underline{v}_1^{(f')}$ and $\underline{v}_2^{(f')}$ onto the direction vector \underline{q} are the two vectors \underline{v}_{1_q} and \underline{v}_{2_q} . The orthographically projected velocity for the pinion is calculated by

$$\underline{v}_{1_q} = \left(\underline{v}_1^{(f')} \cdot \frac{\underline{q}}{|\underline{q}|} \right) \frac{\underline{q}}{|\underline{q}|} \tag{28}$$

and the orthographically projected velocity for the face-gear is calculated by

$$\underline{v}_{2_q} = \left(\underline{v}_2^{(f')} \cdot \frac{\underline{q}}{|\underline{q}|} \right) \frac{\underline{q}}{|\underline{q}|} \tag{29}$$

The sliding speed v_{s_q} is determined by

$$v_{s_q} = \left(\underline{v}_{2_q} - \underline{v}_{1_q} \right) \cdot \frac{\underline{q}}{|\underline{q}|} \tag{30}$$

and the equation for calculating the rolling speed is

$$v_{r_q} = \left(\underline{v}_{2_q} + \underline{v}_{1_q} \right) \cdot \frac{\underline{q}}{|\underline{q}|} \tag{31}$$

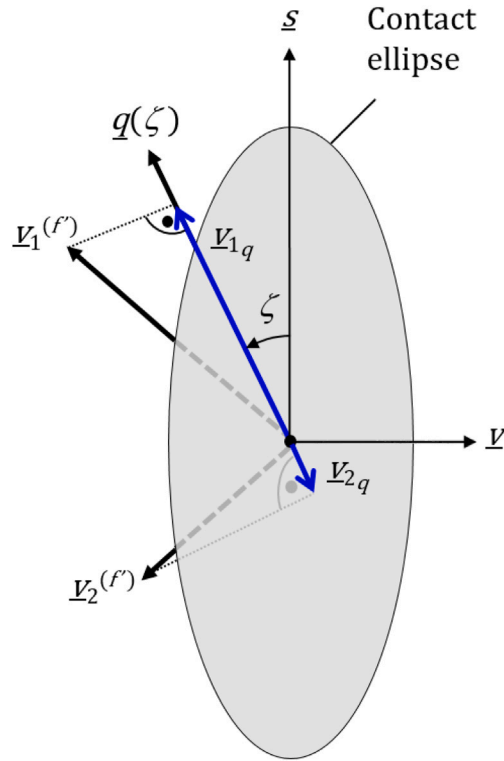


Fig. 7. Contact ellipse and the orthographic projections of the velocity vectors onto the direction vector \underline{q} .

To find the maximum sliding speed $v_{s_{max}}$ at the contact point $r_c^{(f')}$, one of the two sliding velocities $\underline{v}_1^{(f')}$ and $\underline{v}_2^{(f')}$ must simply be subtracted from each other. A projection is not necessary because the relative velocity along the normal vector is zero at the contact point. This maximum sliding velocity is thus at the same time the direction vector \underline{q}_{max} for the maximum sliding speed in the contact ellipse. For the maximum sliding speed $v_{s_{max}}$ it follows

$$v_{s_{max}} = \left| \underline{v}_2^{(f')} - \underline{v}_1^{(f')} \right| \tag{32}$$

Euler's equation can represent the normal curvature of a contact point on a surface Σ_i in any direction, where the subscript i indicates the surface (1...pinion, 2...face-gear). Fig. 8 contains the relevant data for calculating the curvatures in the direction given by the vector \underline{q} .

Using the Euler equation, the curvature of the pinion in the direction \underline{q} is calculated by

$$\kappa_1(\zeta) = \kappa_{1I} \cos^2 \left(\epsilon_1^{(v)} + \frac{\pi}{2} + \zeta \right) + \kappa_{1II} \sin^2 \left(\epsilon_1^{(v)} + \frac{\pi}{2} + \zeta \right) \tag{33}$$

For the curvature of the face-gear the equation is

$$\kappa_2(\zeta) = \kappa_{2I} \cos^2 \left(\epsilon_2^{(v)} + \frac{\pi}{2} + \zeta \right) + \kappa_{2II} \sin^2 \left(\epsilon_2^{(v)} + \frac{\pi}{2} + \zeta \right) \tag{34}$$

where κ_{iI} and κ_{iII} are the respective principal curvatures of the two surfaces. The radius R_q of a cylinders for an equivalent contact between a cylinder and a plane is calculated by

$$R_q = \frac{1}{\kappa_1(\zeta) + \kappa_2(\zeta)} \tag{35}$$

This radius R_q is then used to calculate the coefficient of friction.

4.2. Determination of friction coefficients, friction loss and efficiency

In order to determine the instantaneous efficiency for a pinion rotation angle ϕ_1 , all contact ellipses are divided into M sections parallel to the direction vector \underline{q} . For each section the equivalent unit load $W'^{(m)}$, the equivalent radius R_q , the sliding speed $v_{s_q}^{(m)}$ and the rolling speed $v_{r_q}^{(m)}$ are determined in direction \underline{q} . The subdivision of the contact ellipse is shown schematically in Fig. 9. To calculate the equivalent unit load $W'^{(m)}$, the distance Δs is used, which is oriented orthogonal to the direction \underline{q} .

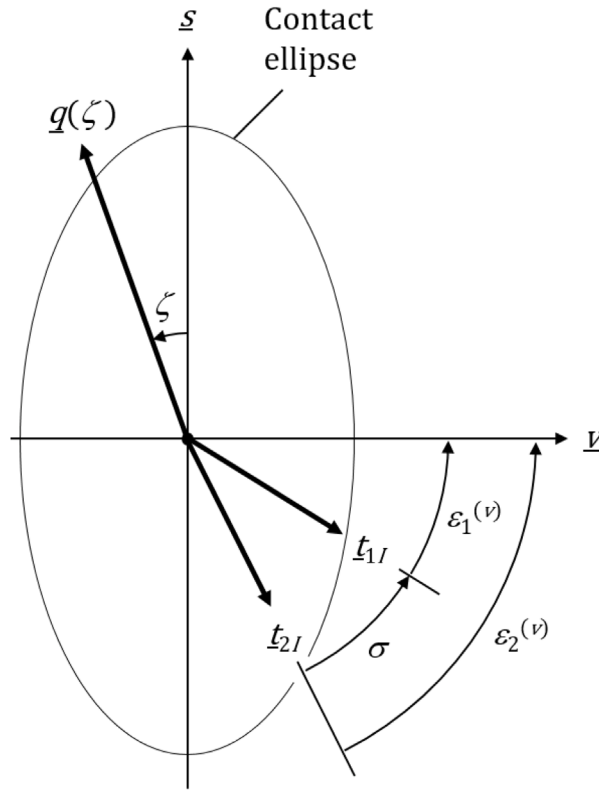


Fig. 8. Contact ellipse and its directions of principal curvatures.

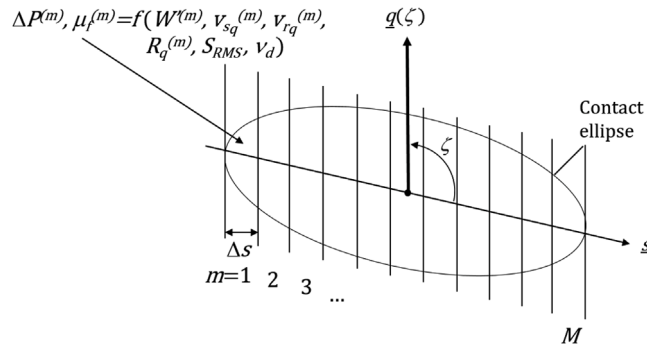


Fig. 9. Subdivision of contact ellipse to calculate the coefficient of friction and the power loss.

Using these parameters as well as the surface roughness S_{RMS} in direction \underline{q} and the lubricant viscosity ν_d , the coefficient of friction $\mu_f^{(m)}$ is determined for each section. With the coefficient of friction $\mu_f^{(m)}$ determined in this way, the power loss $\Delta P^{(m)}(\phi_{1_n})$ in each section can be calculated. It should be noted that the sliding and rolling speeds $v_{sq}^{(m)}$ and $v_{rq}^{(m)}$ in direction of \underline{q} are only used to determine the coefficient of friction $\mu_f^{(m)}$. The friction power loss $\Delta P^{(m)}$ is calculated with the maximum sliding speed $v_{smax}^{(m)}$; thus, the equation for calculating the friction power loss is given by

$$\Delta P^{(m)} = W'^{(m)} \Delta s \mu_f^{(m)} v_{smax}^{(m)} \tag{36}$$

The total power loss $\Delta P(\phi_{1_n})$ is therefore the sum of all power losses across all sections for all contact ellipses for the current pinion rotation angle ϕ_{1_n} . With this total power loss, the instantaneous efficiency for the current pinion rotation angle ϕ_{1_n} is calculated by Eq. (2).

To illustrate the process, a sample wheel set is introduced. The design parameters for the pinion and the face-gear are listed in Table 2. This is a face-gear with an axle offset, which, compared to a face-gear without an axle offset, results in a significantly

Table 2

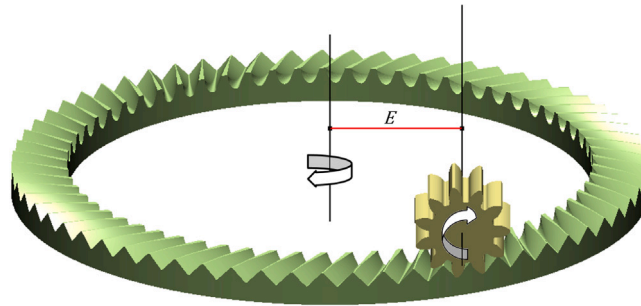
Design parameters of face-gear drive with axle offset to demonstrate the efficiency calculation method.

Design parameter	Symbol	Unit	Value
Pinion number of teeth	N_1	–	11
Shaper number of teeth	N_s	–	13
Face-gear number of teeth	N_2	–	65
Normal module	m_n	mm	1.5
Normal pressure angle	α_n	°	20
Helix angle	β	°	0
Shaft angle	γ_s	°	90
Axle offset	E	mm	–28
Face-gear inner distance	l_{i2}	mm	55.7
Face-gear outer distance	l_{a2}	mm	67.5
Pinion profile shift coefficient	x_p	–	0.325
Shaper profile shift coefficient	$x_s^{(c)}$	–	0.57864
Shift of shaper to produce crowning	$\Delta a^{(c)}$	mm	0.176
Working transv. pressure angle at position of min. backlash	α_w	°	32.76
Torque on pinion	T_1	N m	≤ 10
Rotational speed pinion	n_1	min^{-1}	≤ 3000
Surface roughness	S_{RMS}	μm	0.07
Profile modification		no modification	
Total contact ratio	ϵ_γ	–	1.22

Table 3

Lubricant parameters for 'Castrol Syntrox Universal Plus 75W90' oil [52].

Design parameter	Symbol	Unit	Value
Inlet temperature	T_{oil}	°C	40
Kinematic viscosity at 40 °C under ambient pressure	ν_k	cSt	104
Kinematic viscosity at 100 °C under ambient pressure	ν_k	cSt	15
Density (15 °C)	ρ_m	kg m^{-3}	867

**Fig. 10.** Face-gear drive with axle offset to demonstrate the efficiency calculation method.

higher sliding speed and thus also higher frictional losses. Table 3 lists the lubricant parameters for 'Castrol Syntrox Universal Plus 75W90' oil [52], which are used for the calculations. In Fig. 10, the face-gear drive is shown.

In the case of a face-gear with a shaft angle of $\gamma_s = 90^\circ$ and without axle offset, the maximum sliding velocity, the maximum rolling velocity and the direction of the contact path point almost in the same direction, which in turn corresponds again to the direction of the minor semi-axis of the contact ellipse. Thus, the direction vector \underline{q} to be applied to determine the friction coefficient also points in the same direction.

With increasing axle offset, the directions of the maximum sliding velocity $v_{s,max}$ and the maximum rolling velocity differ increasingly. Since the formula for calculating the coefficient of friction is based on a contact between two cylinders in which the sliding and rolling speeds are collinear, the question thus arises as to which direction \underline{q} is correct for calculating the coefficient of friction. The selection of a face-gear with axle offset has thus been made to determine which direction vector \underline{q} must be applied to calculate the coefficient of friction. In the following, the calculated results for different direction vectors \underline{q} are compared, with the correct direction \underline{q} being determined by means of experiments on a transmission test bench. The results of the experiments are presented in the following section. Fig. 11 shows the contact pattern in terms of the subsequential contact ellipses along the flank and the sliding and rolling velocities along the contact path for the example face-gear according to Table 2. The contact path results from the alignment of the centers of the individual contact ellipses. The tooth flanks engage starting from the tooth tip of the face-gear tooth to the tooth root. The maximum contact pressure occurs at approximately two-thirds of the tooth height of the

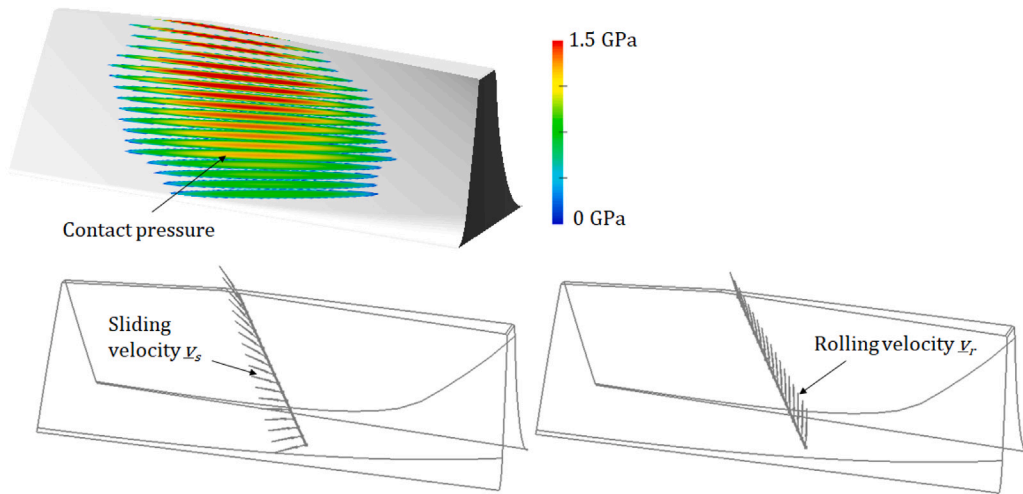


Fig. 11. Contact pattern and sliding and rolling velocities along the contact path for the example face-gear according to Table 2. Pinion torque $T_1 = 10 \text{ N m}$.

face-gear. The calculated contact pressure directly at the tooth tip is unrealistic and is caused by edge contact, which does not occur in this way in the presence of the lubricant film. However, the affected area is very small and contributes only slightly to the overall meshing loss, which is why the influence on the calculated meshing efficiency is low.

The sliding and rolling velocities v_s and v_r are almost perpendicular to one another at the root of the tooth and continue to align their direction towards the tip of the tooth. It is therefore obvious that, depending on the direction \underline{q} in which the coefficients of friction are determined, not only major changes in the speed values $v_{s,q}$ and $v_{r,q}$ but also in the slide-to-roll ratio are to be expected. The following four direction vectors \underline{q} were applied to calculate the coefficient of friction and thus the gear efficiency:

- Vector \underline{q} points in the direction of the rolling velocity v_r .
- Vector \underline{q} points in the direction of the sliding velocity v_s .
- Vector \underline{q} points in the direction of the contact path
- Vector \underline{q} points in the direction of the minor semi-axis of the contact ellipses

The direction of the contact path actually corresponds to the vector sum of the sliding and rolling velocity. Fig. 12 shows the resulting coefficients of friction and the resulting power losses based on Xu's model [30] for these four directions \underline{q} . The absolute values are initially not relevant, rather the differences in the results should be shown. If vector \underline{q} points in the direction of the minor semi-axis of the contact ellipse, very small friction coefficients are determined in part in the middle of the contact ellipse. This is because in these areas the sliding velocity is orthogonal to the direction of the minor semi-axis. This means that pure rolling is present when calculating the coefficient of friction.

The results therefore differ significantly in some cases. This becomes all the more clear when the results for different speeds and torques are considered. Fig. 13 shows the calculated meshing efficiencies η for a pinion torque of $T_1 = 10 \text{ N m}$ and $T_1 = 6 \text{ N m}$.

The influence of torque tends to have a smaller effect on the meshing efficiency. This is not negligible, but at least the influence of the rotational speed, i.e. the resulting rolling and sliding speed, seems to be more important. Unfortunately, it is difficult to determine from theory the correct direction \underline{q} to calculate the coefficient of friction. The formula for determining the coefficient of friction rather indicate a stronger influence of the rolling speed, as this has a higher weight in the respective equation than the sliding speed. But even if the direction of the rolling speed seems more plausible, a more reliable confirmation is required. Therefore, experiments were carried out on a transmission test bench, which is the content of the following section.

5. Experimental validation

The model presented in the previous section for calculating the friction loss in the EHL contact has not yet been validated for use with face-gears. Precisely because the calculated power loss is also strongly dependent on the direction \underline{q} for determining the friction coefficient, a validation of the model on the basis of test bench tests is essential. In this section the results of the theoretical model are compared with results from transmission test bench tests. Based on the measurement results, conclusions can be drawn about a suitable evaluation direction.

5.1. Experimental setup, test bench and test gears

The test runs were carried out on the transmission test bench at the Haute école d'ingénierie et d'architecture Fribourg, Switzerland. This test bench is designed to be very rigid and equipped with precise measurement technology. The test setup consists

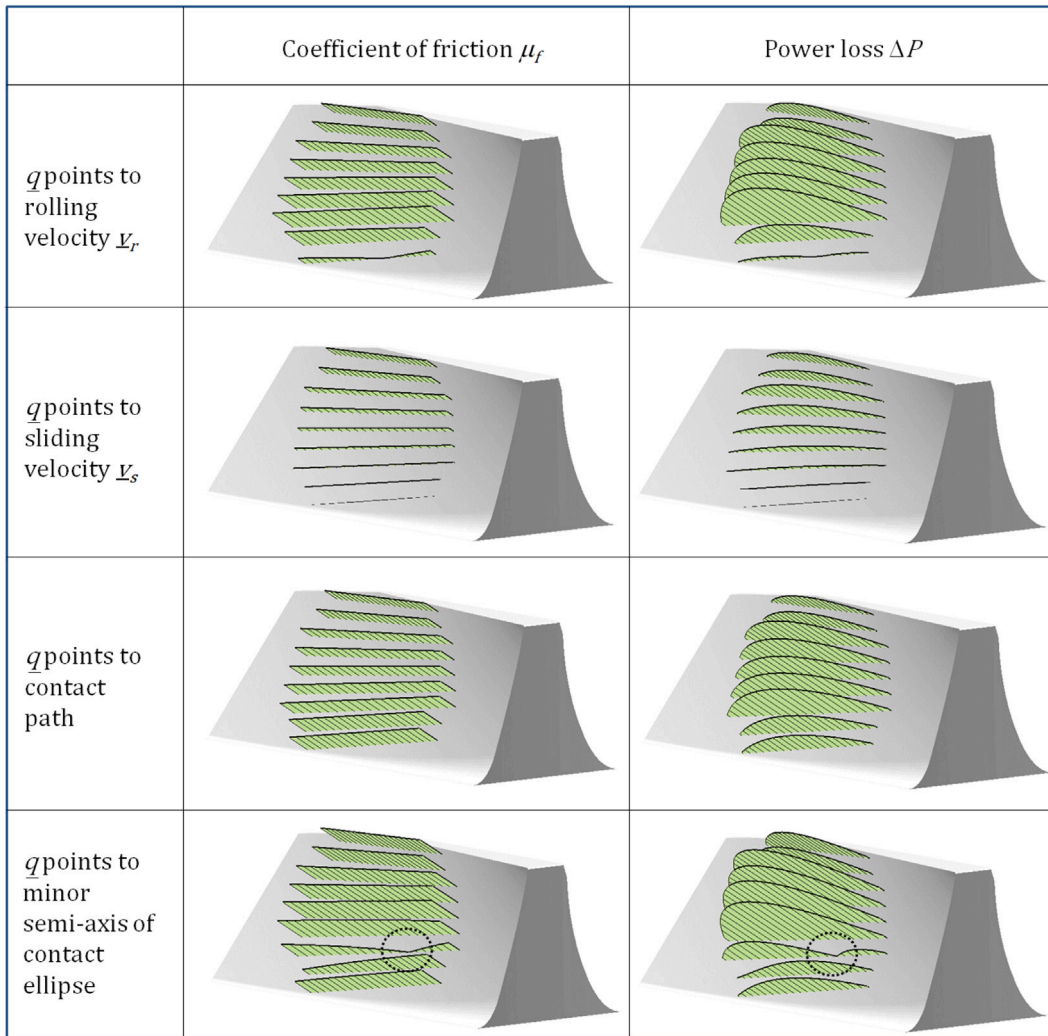


Fig. 12. Resulting coefficients of friction (left) and the resulting power losses (right) based on Xu's model [30] for different directions \underline{q} . From top to bottom: Vector \underline{q} points in the direction of the rolling velocity \underline{v}_r , vector \underline{q} points in the direction of the sliding velocity \underline{v}_s , vector \underline{q} points in the direction of the contact path, vector \underline{q} points in the direction of the minor semi-axis of the contact ellipses. The values are plotted for nine angular positions of the pinion along the major semi-axes of the corresponding contact ellipses. The circles in the lowest column indicate the area in which the sliding velocity is orthogonal to the direction of the minor semi-axis. In this case, this means that there is pure rolling when calculating the coefficient of friction.

of a drive motor, the gearbox to be tested and a brake motor. The torques are measured on the two shafts between the motor and the gearbox. In addition, the angular positions of the two shafts are recorded by measurement, but this is not important for calculating the efficiency. By multiplying the respective torque and the respective speed, the power can be calculated on the input and output side. The difference between the two quantities then corresponds to the total power loss of the transmission ΔP_t ,

$$\Delta P_t = P_{in} - P_{out} = T_1 \frac{2\pi n_1}{60} - T_2 \frac{2\pi n_2}{60} \tag{37}$$

where T_1 is the measured torque on the pinion shaft, T_2 is the measured torque on the face-gear shaft and n_1 and n_2 are the corresponding rotational speeds in min^{-1} . Fig. 14 shows the hardware part of the test bench. The essential key data are listed in Table 4.

The examined gears for the test series correspond to those from Table 2 of the last section. It is therefore a spur pinion with an associated face-gear with an axle offset. No profile modifications were applied to both gears. As usual for spur gears, the pinion was produced by hobbing. Since the face-gear is a unique piece and no existing tool was available, it was milled on a 5-axis machine tool. Both gears are made of hardened steel. The pinion consists of case-hardened 16MnCr5 (1.7131, 0.7-0.9/56-60HRC), case-hardened 18CrNiMo7-6 (1.6587, 0.7-0.9/56-60HRC) is used for the face-gear. Fig. 15 shows the manufactured test gears mounted on their shafts. The pinion is attached to the drive shaft by means of a conical press connection, the face-gear sits with a slight overlap fit on the output shaft and is bolted to it on the back.

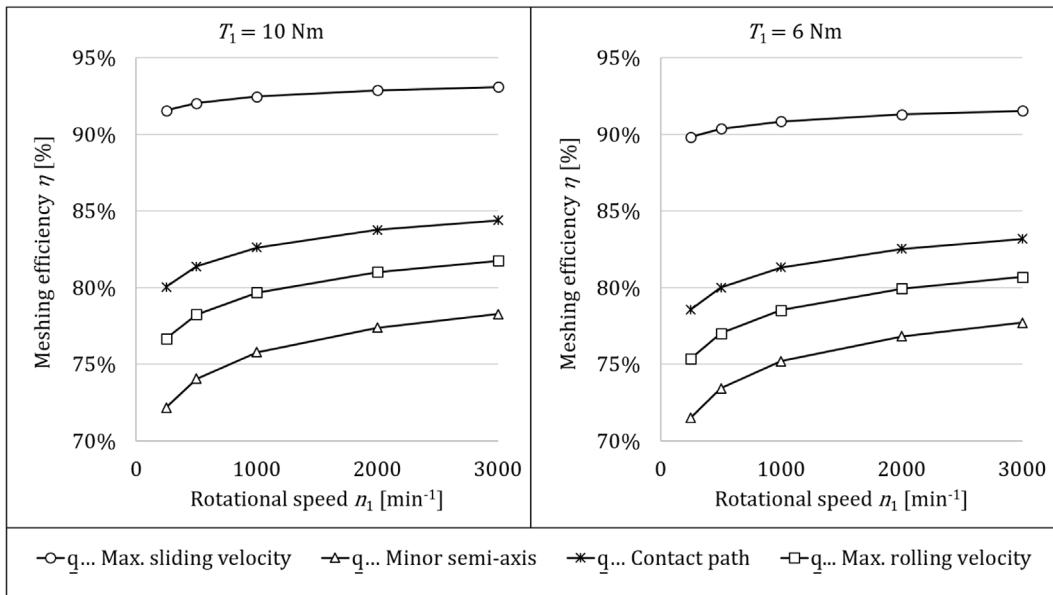


Fig. 13. Calculated meshing efficiency η depending on the direction q used to calculate the coefficient of friction, the applied formula for the coefficient of friction and the pinion rotational speed n_1 for a constant pinion torque of $T_1 = 10 \text{ Nm}$ (left), $T_1 = 6 \text{ Nm}$ (right) and a surface roughness of $S_{RMS} = 0.07 \text{ }\mu\text{m}$.

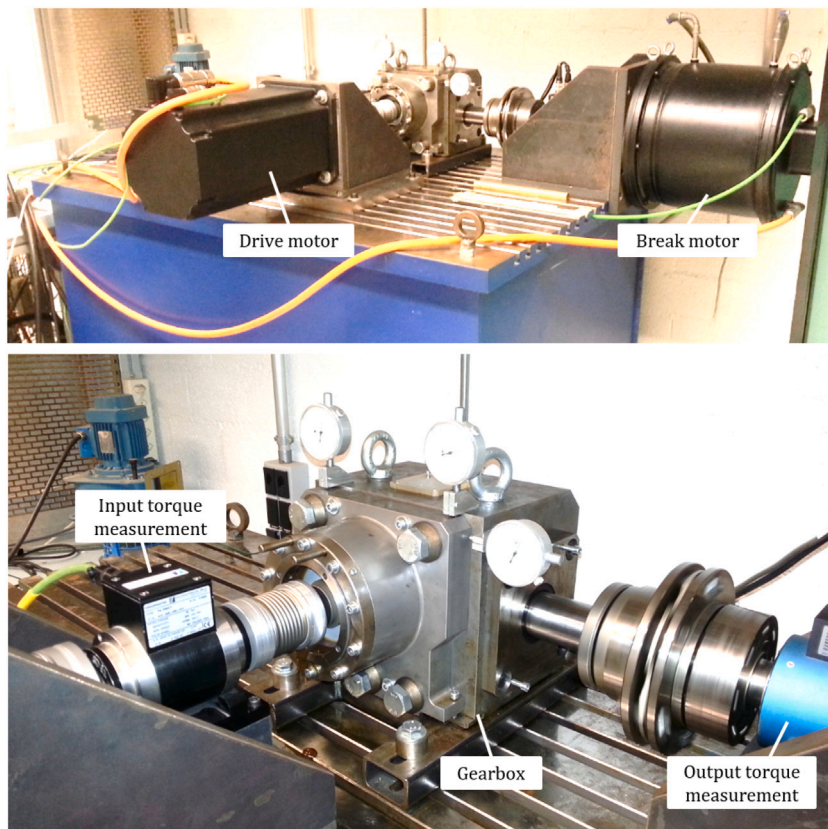


Fig. 14. The transmission test bench at the Haute école d'ingénierie et d'architecture Fribourg, Switzerland, used to validate the efficiency model.

Table 4

Key data of the transmission test bench at the Haute école d'ingénierie et d'architecture Fribourg, Switzerland, used to validate the efficiency model.

Drive side	
Motor	B & R Automation 8LSA85
Rotational speed	1500 min ⁻¹
Torque	77 Nm (max. 94 Nm)
Torque sensor	Magtrol Torquemaster TM 309/11
Torque	20 Nm
Max. combined error of linearity and hysteresis	±0.1%
Output side	
Motor	Torque Motor B & R Automation 8LTJC6
Rotational speed	80 min ⁻¹
Torque	695 Nm (max. 714 Nm)
Torque sensor	MTS KSM4503A1KL000
Measuring ranges	0...1000 Nm (0...200 Nm)
Max. combined error of linearity and hysteresis	±0.1% (±0.2%)
Rotational speed	max. 8000 min ⁻¹
Oil temperature measurement	
Sensor	PT100
Location	Oil bath

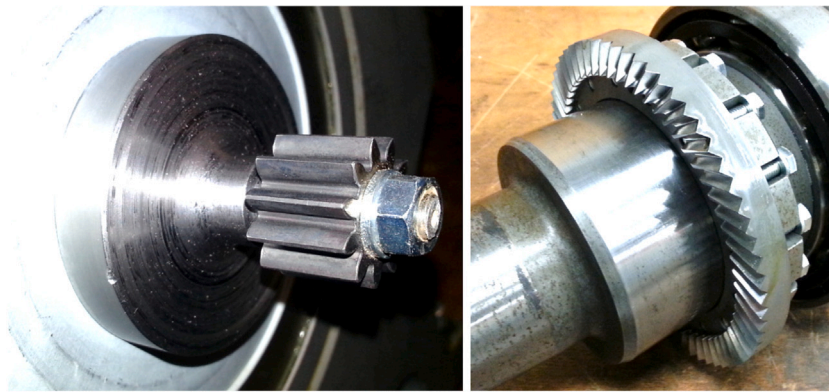


Fig. 15. Test gears to measure the efficiency of a face-gear stage: (left) pinion mounted on the drive shaft; (right) Face-gear mounted on the output shaft.

The face-gear shaft is supported on both sides of the gear by two spindle bearings. Radial seal rings are installed at the shaft ends. The face-gear is lubricated by splash lubrication, with approximately one quarter of the face-gear in the oil bath. The bearings are thus lubricated with the same oil. As a result of the realized axle offset, the pinion shaft is vertically offset relative to the face-gear shaft. The pinion itself is therefore not in the oil bath. The pinion shaft is supported by two grease-lubricated tapered roller bearings in an O arrangement and sealed by Nilos rings. Fig. 16 shows the schematic structure of the transmission.

Since the face-gear was milled on a 5-axis machine tool, checking the flank topography on a gear measuring machine is necessary. As a result, it can be stated that the tooth flank topography is reproduced well. The tooth flanks are thickened by approximately 10 µm on the inside while the tooth flanks are approximately 10 to 15 µm thinner on the outside. Such a profile is common when there is an offset in the axial direction of the face gear, either during manufacture or during measurement. In any case, these deviations can be easily compensated by a small shift of the pinion in the direction of the face-gear rotation axis during installation, but also in simulation.

The surface roughness required for the efficiency model was determined for both gears using a tactile roughness measuring device from Taylor Hobson. The measurement was carried out in accordance with the standards DIN EN ISO 4288 [53] and DIN EN ISO 3274 [54]. However, the tooth heights are less than the evaluation length required by the standard for determining the roughness. Therefore, the measuring sections over the tooth height, and thus also the evaluation lengths for determining the roughness, had to be reduced by 22.5% for the face-gear and by 35% for the pinion. The measured roughness values vary in the usual range of approximately 15 to 20%, the roughness along the profile of the pinion being approximately $S_{RMS} = 0.59$ µm and the roughness along the flank lines of the pinion being approximately $S_{RMS} = 0.36$ µm. For the face-gear, a roughness of approximately $S_{RMS} = 0.61$ µm was determined along the profile, a value of approximately $S_{RMS} = 0.35$ µm results along the flank lines. The surface roughness in both directions also corresponds to the directions with the maximum and the minimum roughness. Thus, the roughness can be calculated in any direction along the flank.

Table 5 summarizes the essential parameters and settings for the tests carried out. The design parameters of the gears correspond to the values in Table 2. It should be noted that the maximum possible rotational speed is limited by the brake motor. The bearings

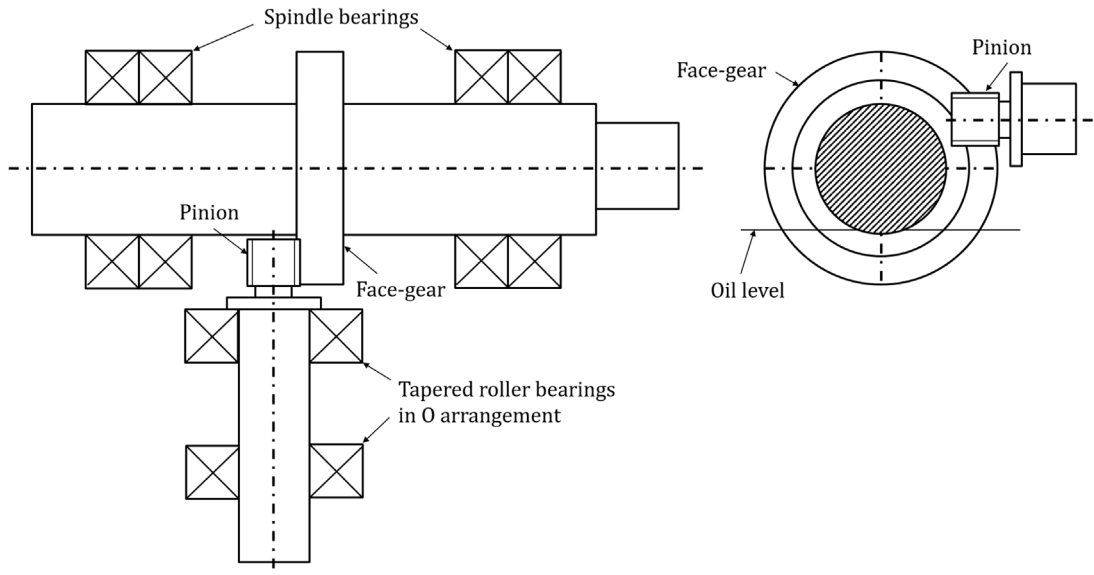


Fig. 16. Schematic structure of the transmission: (left) Top view; (right) Side view in the direction of the face-gear shaft.

Table 5
Parameters and settings for the efficiency tests.

	Symbol	Unit	Value
Load and rotational speed			
Torque on pinion	T_1	Nm	~ 10
Corresponding max. contact pressure	p_{max}	MPa	~ 1800
Rotational speed pinion	n_1	min ⁻¹	300 ... 1000
Lubricant			
Castrol Syntrox Universal Plus 75W90			
Oil temperature	T_{oil}	°C	~ 20

installed on the pinion shaft are designed for bigger forces. Since a minimal load is required to estimate the power loss in the bearings, small pinion torques could be used, but a reliable back calculation of the gear meshing efficiency is not possible. Thus, the test series were run at a torque of $T_1 = 10$ N m, which also ensures the usual flank pressures for gear wheels made of hardened material.

5.2. Determination of the meshing efficiency

Since the measured variables only provide conclusions about the total loss ΔP_t of the transmission, the meshing power loss ΔP must be determined by calculation. The total loss is made up of the following partial losses: The bearing losses, the oil churning and windage losses, the meshing loss and the sealing losses. Due to the low rotational speed, the windage losses can be neglected. Furthermore, the pinion is not in the oil bath, which is why only oil churning losses from the face-gear have to be taken into account. The drive shaft is sealed with Nilos sealing rings. After a running-in period, these practically no longer show any significant losses, which is why these can also be neglected in the calculation.

As a result, the total power loss is made up of the sum of the bearing losses of the drive shaft, the meshing loss, the oil churning loss of the face-gear and the bearing and sealing losses of the output shaft

$$\Delta P_t = \Delta P_{bearing_1} + \Delta P + \Delta P_{ch_2} + \Delta P_{bearing_2} + \Delta P_{seal_2} \quad (38)$$

The oil churning loss of the face-gear and the sealing losses can be calculated directly as they are load-independent. The power losses in the bearings, however, depend on the forces acting on them. Depending on the losses in the pinion bearings, there is a resulting torque acting on the pinion. The corresponding acting gear forces, whereby the oil churning loss of the face-gear and the sealing losses are also taken into account, in turn determine the acting bearing forces. To take this relationship into account, the individual power losses in the bearings are determined iteratively. In the first step, the bearings are assumed to be loss-free, with which the acting bearing forces are calculated via the resulting gear forces. With the bearing forces determined in this way, the power losses in the bearings can now be calculated, which leads to a new torque at the pinion and thus results in new gear forces. This in turn leads to the calculation of new bearing forces, which in turn lead to corresponding new power losses in the bearings.

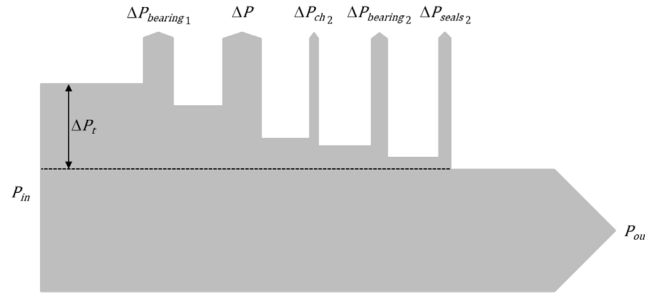


Fig. 17. Total power loss ΔP of the transmission as the sum of input shaft bearing losses $\Delta P_{bearing_1}$, meshing loss ΔP , face-gear oil churning loss ΔP_{ch_2} , output shaft bearing losses $\Delta P_{bearing_2}$ and output shaft sealing losses ΔP_{seal_2} .

The losses in the bearings are thus iteratively determined by always using the calculated bearing forces from the previous iteration. This iterative process is repeated until the bearing forces and power losses of two successive iterations are practically identical, which is the case after only a few iterations. The chain of the individual power losses is shown schematically in Fig. 17.

Based on Eq. (38), the meshing loss can be calculated as follows:

$$\Delta P = \Delta P_t - \Delta P_{bearing_1} - \Delta P_{ch_2} - \Delta P_{bearing_2} - \Delta P_{seal_2} \quad (39)$$

The total power loss is determined from the torque measurements and calculated by Eq. (38). The power loss in the bearings can be calculated using the correlations provided by the bearing manufacturers. Bearings from SCHAEFFLER are used for the test bed. Therefore, the bearing losses were calculated with the available online tool from SCHAEFFLER “BEARINX-online Easy Friction” [55]. In general, the losses in the bearings depend largely on the forces applied, the type of load, the rotational speed, the installation tolerances, the lubricant used, the pre-load and the bearing temperature.

According to Boness [56], the oil churning torque T_{ch} can be expressed as

$$T_{ch} = 0.5 \rho_m \omega^2 r^3 S_m C_m \quad (40)$$

where ρ_m is the density of the lubricant, ω is the rotational speed of the shaft, r is the pitch radius of the gear, S_m is the submerged surface area and C_m is the dimensionless drag torque. For the oil churning power loss P_{ch} it follows

$$\Delta P_{ch} = 0.5 \rho_m \omega^3 r^3 S_m C_m \quad (41)$$

The formula from Changenet and Vexel [57,58] to estimate the dimensionless drag torque C_m of a gear is given by

$$C_m = \begin{cases} 1.366 \left(\frac{h_d}{2r} \right)^{0.45} \left(\frac{V_0}{8r^3} \right)^{0.1} Fr^{-0.6} Re^{-0.21}, & Re_c < 6000 \\ 3.644 \left(\frac{h_d}{2r} \right)^{0.1} \left(\frac{V_0}{8r^3} \right)^{-0.35} Fr^{-0.88} \left(\frac{w}{2r} \right)^{0.85}, & Re_c > 9000 \end{cases} \quad (42)$$

where h_d is the gear immersion depth, w is the tooth width, Fr is the Froude number, Re is the Reynolds number and Re_c is the critical Reynolds number. There are some other formulae for estimating oil churning loss in the literature. For example, Xu [30] uses the formulae provided by the British Standard BS ISO/TR 14179 [59] and Dong et al. [29] use the formula from Boness [56] to estimate the oil churning losses on a face-gear. All three equations were tried out for the test conditions, and it was shown that the oil churning loss at the relatively low speed of the face-gear shaft is very low compared to the other losses and can practically be neglected. The effect of oil trapping between the meshing teeth is not taken into account in the calculations.

With regard to the radial shaft seals used, the manufacturers only provide sparse information on the losses; this applies above all to low rotational speeds. Engelke [60] experimentally investigated the friction loss in radial shaft seals and set up a model to calculate the loss. The measurement results from Engelke [60] are used to estimate the sealing losses in the transmission test bench. The losses are quite low due to the low speed of the shaft and, moreover, the losses in the seals are also small compared to the other losses. A rough estimate of the sealing losses is therefore permissible in this case. Following equation was created from the curves provided by Engelke in order to estimate the torque T_{seal} up to a peripheral speed of $v = 1 \text{ m s}^{-1}$:

$$T_{seal} = \frac{0.06}{[\text{m s}^{-1}]} v F_r R_{shaft} \quad (43)$$

where F_r is the radial pretensioning force of the seal pressing on the shaft, and R_{shaft} is the radius of the shaft. Based on Engelke’s results, a radial line force of 85 N m^{-1} related to the circumference of the shaft can be assumed for the seals actually installed in the test bed, with which the radial force F_r can be calculated for each of the seals. It should be noted that this rough assumption is only applicable because the speed of the shaft is low and, moreover, the losses in the seals are small compared to the other losses.

Finally, to calculate the meshing efficiency from the experiments, it follows

$$\eta = 1 - \frac{\Delta P}{P_{in} - \Delta P_{bearing_1}} \quad (44)$$

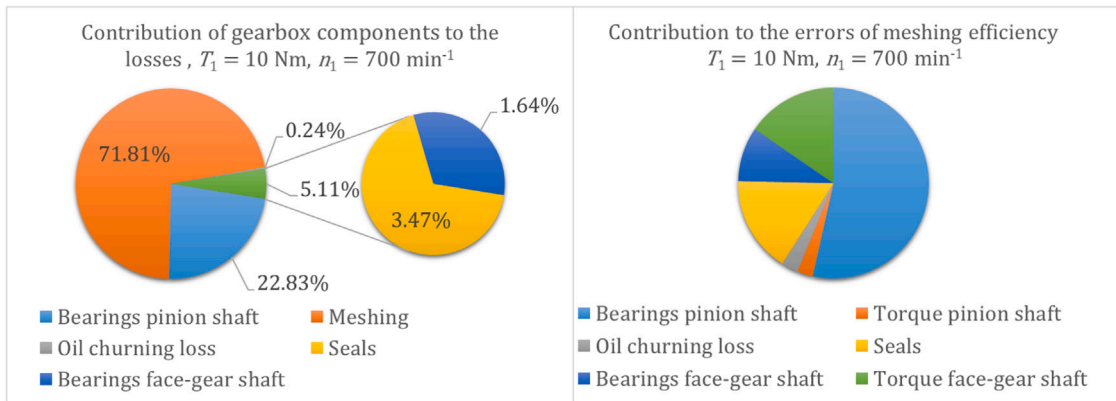


Fig. 18. Contribution of the individual components to the total power loss and the measurement errors. The proportion of power loss of pinion bearings is comparatively high (left) and produces the highest error when calculating the meshing efficiency (right).

5.3. Results

In the following, the measurement results are compared with the calculated values for the four different directions \underline{q} . There are a few more comments to make: The transmission test bench was originally designed for a very high transmission ratio. Therefore, the nominal speed of the brake motor is quite low at $n_2 = 80 \text{ min}^{-1}$. Since the power required for the brake motor in the test series is comparatively low, the speed could be increased to approximately $n_2 = 160 \text{ min}^{-1}$, which corresponds to a pinion speed of $n_1 = 1000 \text{ min}^{-1}$. Higher speeds are not possible with this test bench. The bearings installed on the pinion shaft are designed for bigger forces. Since a minimal load is required to estimate the power loss in the bearings, small pinion torques could be used, but a reliable back calculation of the gear meshing efficiency is not possible. As shown in Fig. 13, the influence of the pinion torque on the meshing efficiency is quite small. Thus, the test series were run at a torque of $T_1 = 10 \text{ Nm}$, which also ensures the usual flank pressures for gear wheels made of hardened material. An increase of the torque is not possible, as this would exceed the strength of the shaft at the tapered press fit of the pinion.

The Gaussian law of error propagation was used for the error estimation. In addition to the known measuring device errors, which have the least influence on the resulting overall error for the measured efficiency, the errors for the losses in the bearings, the seals and due to oil churning must be estimated. With regard to the losses in the seals and due to oil churning, it is conservatively assumed that these have an error of 50%. Losses in seals and oil churning losses are generally very small at low speeds compared to bearing and meshing losses. Thus, even this assumed high error has little influence on the results. However, at higher speeds, which cannot be realized with the test bench used, the influence of the seal losses and the oil churning losses would increase. For the bearings of both shafts, an error of about 10% of the average calculated torque loss of each shaft is assumed due to the friction in the bearings. The main part of the error is based on the uncertain bearing temperature, which affects the viscosity of the lubricant. The temperature on the housing near the bearings could be measured, but the temperature in the bearing itself can only be estimated. It is assumed that the actual bearing temperature deviates from the assumed bearing temperature by 5K. A smaller part of the error is due to the axial pre-load of the bearings, which is not precisely known due to the error of the tightening torque when mounting the shaft. The bearings installed in the test bench are quite large and allow much larger forces than those encountered in this test campaign. Due to the size of the bearings, the losses are generally quite large, which is why the error of the bearing losses have a correspondingly large influence on the error of the calculated meshing efficiency. Fig. 18 shows the influence of the different components of the whole gearbox on the total power loss as well as their contribution to the error of the determined meshing efficiency η .

The test bench is located in the basement, where a constant temperature prevails over the entire measurement period. The oil temperature is measured in the oil bath inside the housing. Due to the rather low power and the massive construction of the gearbox housing, which can therefore absorb a lot of heat, the temperature only increased by 0.2K over the measured period. It should be noted, however, that oil viscosity at these low temperatures is quite sensitive to temperature changes. A change in the oil inlet temperature by 2K leads to a change in the calculated gear efficiency by 2%.

Fig. 19 shows the experimentally determined results with calculated results obtained for the different four directional vectors \underline{q} . The results show that the direction \underline{q} , which points in the direction of the contact path, is correct to calculate the friction coefficient. The direction \underline{q} , which points in the direction of the maximum sliding velocity, leads to a significant overestimation of the meshing efficiency. If the coefficient of friction is determined in the direction \underline{q} , which points in the direction of the minor semi-axis of the contact ellipse, on the other hand, the meshing efficiency is significantly underestimated. An underestimation of the meshing efficiency also results if the coefficient of friction is determined in the direction of the maximum rolling speed, although the deviations compared with the measured values are much smaller.

With the direction \underline{q} , not only the rolling and sliding velocities change, but also the curvatures, surface roughness and acting forces. Thus, the greater differences in the results for the different four directions \underline{q} are logical, which makes it possible to determine

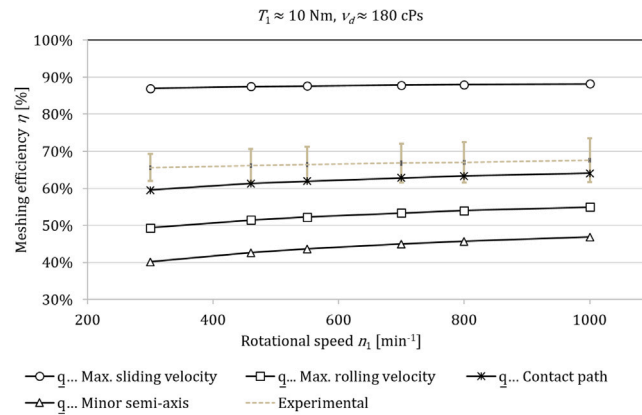


Fig. 19. Comparison of calculated meshing efficiencies η with experimental results for a pinion torque of $T_1 = 10$ N m and a dynamic viscosity of the lubricant of $\nu_d = 180$ cPs. The calculated meshing efficiencies are obtained for the different four directional vectors \underline{q} .

the correct direction \underline{q} for calculating the coefficient of friction. However, the decisive factor is probably not only the direction of the contact path, but rather the question of how the sliding and rolling velocities relate to each other. In the future, the question could therefore arise whether the angle between the two velocities should not be taken into account in order to build a more complex model.

Although the simulation results for the vector \underline{q} in the direction of the contact path, where this direction actually also corresponds to the vector sum of rolling and sliding velocity, agree quite well with the experimentally determined values, it can be seen that the slopes of the two curves do not match exactly. As the speed decreases, the differences become increasingly larger; the calculated meshing efficiency falls more sharply with decreasing speed than the corresponding experimentally determined value. That the differences tend to increase with decreasing speed is not surprising, since asperity contact increases and this has a sensitive influence on the resulting power loss. In addition, the formula according to Xu is in the parameter boundary range at the lower speeds, which were taken into account in his investigations. A more detailed analysis is not possible even considering the estimated error of the experimental results, but overall the agreements are quite good, with increasing convergence between experiment and simulation with increasing speed. Experimental matching of the simulation for even higher speeds would be desirable, which may be the content of future research.

6. Influence of the main parameters on the meshing efficiency

In order to investigate the influence of the main parameters on the meshing efficiency η , the values for surface roughness S_{RMS} , dynamic viscosity ν_d , pinion torque T_1 and alignment errors $\Delta\gamma$, ΔE , Δa were each systematically varied for the example face-gear drive according to Table 2, and the meshing efficiency was thus determined in each case, using the vector \underline{q} pointing in the direction of the contact path to determine the friction coefficients. Fig. 20 shows the calculated meshing efficiency versus pinion speed for varied values of surface roughness, dynamic viscosity and pinion torque.

The influence of the individual parameters on the meshing efficiency can be summarized as follows:

- The rotational speed of the pinion n_1 has a considerable influence on the meshing efficiency. With increasing speed, the efficiency increases, whereby the most significant changes are found in the lower speed range.
- With the increase of the surface roughness S_{RMS} , the meshing efficiency decreases considerably. This influence is slightly higher towards lower speeds.
- The dynamic viscosity ν_d is also one of the parameters with a major influence on the meshing efficiency. This increases with decreasing viscosity. Since the dynamic viscosity depends mainly on the oil temperature, higher oil temperatures therefore lead to increased meshing efficiency.
- An increase in pinion torque T_1 leads to a small increase in meshing efficiency, which means that torque can be categorized as a parameter with a minor influence.
- The meshing power loss increases significantly with the sliding speed. Thus, an axle offset E of the face-gear is definitely a parameter which leads to a significant reduction of the meshing efficiency.
- Calculations with different alignment errors ($\Delta\gamma$, ΔE , Δa), whereby the contact pattern always remains within the flank, show that this results in only minor changes in the meshing efficiency of a maximum of $\pm 1\%$.
- The meshing efficiency is mainly dependent on the sliding speed. An axle offset leads to an increasing component of the sliding velocity in the direction of the flank lines, which becomes dominant with increasing axle offset. Larger axle offsets thus lead to a significant reduction in the meshing efficiency.

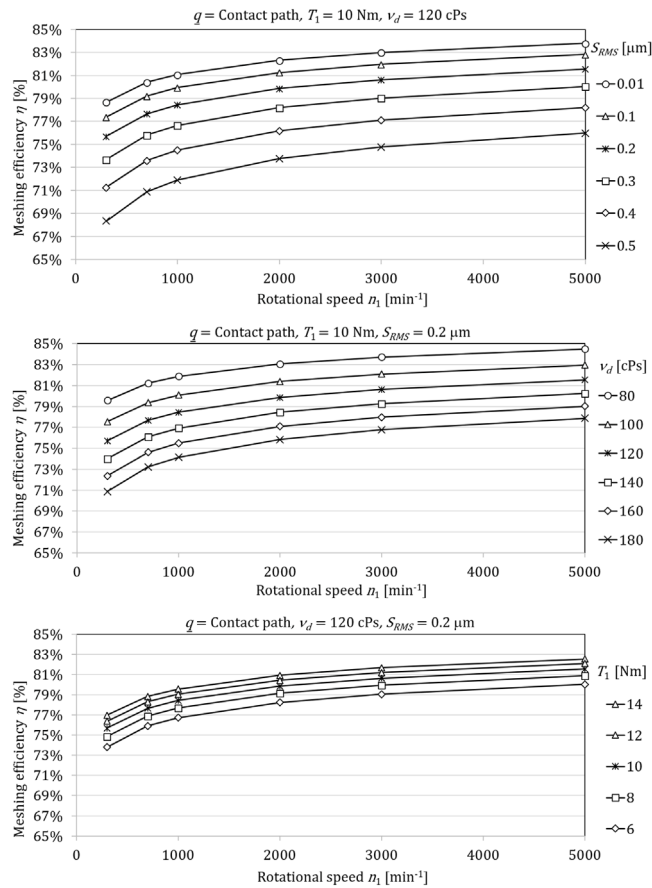


Fig. 20. Calculated meshing efficiencies η obtained for the vector q pointing in the direction of the contact path for varied parameters: (top) Varied surface roughness S_{RMS} ; (middle) Varied dynamic viscosity ν_d ; (bottom) Varied pinion torque T_1 .

7. Conclusions

The estimation of the meshing efficiency of a face-gear stage can be done using the physics based formulae of Xu [30] for calculating the coefficient of friction in elastohydrodynamic contact. If the contact path and the associated contact ellipses are calculated based on a contact analysis, corresponding coefficients of friction and thus the power loss can be calculated by discretizing these contact ellipses and setting up substitute models for these segments. Measurements on a transmission test bench have shown that the meshing efficiency can be well estimated with the formula of Xu for a face-gear with axle offset at lower speeds, if the parameters for calculating the coefficient of friction are determined in the direction of the contact path.

The estimation of meshing efficiency is not only helpful with regard to the optimization of a face-gear with respect to friction losses, but also enables comparisons with the achievable efficiencies of other gear types such as bevel gears, hypoid gears and worm gears, thus supporting the appropriate selection of the gear type for a specific application.

The experimental validation at higher speeds as well as more precise investigations regarding the directions of sliding and rolling velocities also in relation to the resulting contact ellipses could be the core of future research. Further series of measurements are required for this purpose, whereby different face-gears could be used, each with a different axle offset.

Declaration of competing interest

The authors declare that they have no known competing financial interests or personal relationships that could have appeared to influence the work reported in this paper.

Acknowledgments

Funding: This work was supported by the Commission for Technology and Innovation (CTI), Switzerland [project no. 17252.1 PFIW-IW]. The authors would like to thank Prof. Sebastian Leopold and Prof. Nicolas Rouvé from the Haute école d'ingénierie et d'architecture Fribourg for allocation of the gear test rig and their strong contribution and support regarding the performed experiments.

References

- [1] F. Reuleaux, Friction in tooth gearing, *Trans. ASME* 8 (9) (1886) 45–85.
- [2] K. Martin, A review of friction predictions in gear teeth, *Wear* 49 (2) (1978) 201–238.
- [3] T. Yada, Review of gear efficiency equation and force treatment, *JSME Int. J. Ser. C Dynam. Control Robotics Des. Manuf.* 40 (1) (1997) 1–8.
- [4] D. Mba, P. Heingartner, Determining power losses in the helical gear mesh; case study, *Gear Technol.* (2005).
- [5] T.T. Petry-Johnson, A. Kahraman, N. Anderson, D. Chase, An experimental investigation of spur gear efficiency, *J. Mech. Des.* 130 (6) (2008).
- [6] T. Yada, The measurement of gear mesh friction losses, *ASME Paper (72-PTG)* (1972) 35.
- [7] C. Naruse, S. Haizuka, R. Nemoto, K. Kurokawa, Studies on frictional loss, temperature rise and limiting load for scoring of spur gear, *Bull. JSME* 29 (248) (1986) 600–608.
- [8] C. Naruse, S. Haizuka, R. Nemoto, H. Takahashi, Influences of tooth profile on frictional loss and scoring strength in the case of spur gears, in: *JSME International Conference on Motion and Power Transmissions*, 1991, pp. 1078–1083.
- [9] H. Mitzutani, Y. Ishikawa, Power loss of long addendum spur gears, *VDI-Ber.* 1230 (1996) 83–96.
- [10] D.C. Talbot, A. Kahraman, A. Singh, An experimental investigation of the efficiency of planetary gear sets, *J. Mech. Des.* 134 (2) (2012).
- [11] A. Vaidyanathan, An Experimental Investigation of Helical Gear Efficiency (Ph.D. thesis), The Ohio State University, 2009.
- [12] C. Denny, *Mesh Friction in Gearing*, AGMA, 1998.
- [13] J. Pedrero, M. Pleguezuelos, et al., Simplified calculation method for the efficiency of involute spur gears, in: *ASME 2009 International Design Engineering Technical Conferences and Computers and Information in Engineering Conference*, American Society of Mechanical Engineers Digital Collection, 2009, pp. 131–138.
- [14] M. Pleguezuelos, J. Pedrero, M. Sánchez, Simplified calculation method for the efficiency of involute helical gears, in: *New Trends in Mechanism Science*, Springer, 2010, pp. 217–224.
- [15] Y. Michlin, V. Myunster, Determination of power losses in gear transmissions with rolling and sliding friction incorporated, *Mech. Mach. Theory* 37 (2) (2002) 167–174.
- [16] J.A. Misharin, Influence of the friction conditions on the magnitude of the friction coefficient in the case of rolling with sliding, *Instn. Mech. Engrs., Proc. Int. Conf. Gearing* 159 (1958) 1958.
- [17] G. Benedict, B. Kelley, Instantaneous coefficients of gear tooth friction, *ASLE Trans.* 4 (1) (1961) 59–70.
- [18] Y.N. Drozdov, Y.A. Gavrikov, Friction and scoring under the conditions of simultaneous rolling and sliding of bodies, *Wear* 11 (4) (1968) 291–302.
- [19] J. O'donoghue, A. Cameron, Friction and temperature in rolling sliding contacts, *ASLE Trans.* 9 (2) (1966) 186–194.
- [20] P. Ku, H. Staph, H. Carper, Frictional and thermal behaviors of sliding-rolling concentrated contacts, *ASME J. Lubr. Technol.* 100 (1) (1978) 121–128.
- [21] B. Kelley, A. Lemanski, Paper 11: lubrication of involute gearing, in: *Proceedings of the Institution of Mechanical Engineers, Conference Proceedings*, 182, (1) SAGE Publications Sage UK: London, England, 1967, pp. 173–184.
- [22] K.L. Johnson, J. Tevaarwerk, Shear behaviour of elastohydrodynamic oil films, *Proc. R. Soc. Lond. Ser. A Math. Phys. Eng. Sci.* 356 (1685) (1977) 215–236.
- [23] N.E. Anderson, S.H. Loewenthal, Effect of geometry and operating conditions on spur gear system power loss, *ASME J. Mech. Des.* 103 (1) (1981) 151–160.
- [24] N.E. Anderson, S.H. Loewenthal, Design of spur gears for improved efficiency, *ASME J. Mech. Des.* 104 (4) (1982) 767–774.
- [25] N.E. Anderson, S.H. Loewenthal, Comparison of spur gear efficiency prediction methods, *NASA-CP-2210*, 1983.
- [26] N.E. Anderson, S.H. Loewenthal, Efficiency of nonstandard and high contact ratio involute spur gears, *ASME J. Mech. Transm. Autom. Design* 108 (1) (1986) 119–126.
- [27] N.E. Anderson, S.H. Loewenthal, J.D. Black, An analytical method to predict efficiency of aircraft gearboxes, *ASME J. Mech. Transm. Autom. Design* 108 (3) (1986) 424–432.
- [28] P. Heingartner, D. Mba, Determining power losses in helical gear mesh: case study, in: *ASME 2003 International Design Engineering Technical Conferences and Computers and Information in Engineering Conference*, American Society of Mechanical Engineers Digital Collection, 2003, pp. 965–970.
- [29] H. Dong, Z.-Y. Liu, L.-L. Duan, Y.-h. Hu, Research on the sliding friction associated spur-face gear meshing efficiency based on the loaded tooth contact analysis, *PLoS One* 13 (6) (2018) e0198677.
- [30] H. Xu, Development of a Generalized Mechanical Efficiency Prediction Methodology for Gear Pairs (Ph.D. thesis), The Ohio State University, 2005.
- [31] C. Ratanasumawong, P. Asawapichayachot, S. Phongsupasamit, H. Houjoh, S. Matsumura, Estimation of sliding loss in a parallel-axis gear pair, *J. Adv. Mech. Des. Syst. Manuf.* 6 (1) (2012) 88–103.
- [32] C. Yenti, S. Phongsupasamit, C. Ratanasumawong, Analytical and experimental investigation of parameters affecting sliding loss in a spur gear pair, *Eng. J.* 17 (1) (2013) 79–94.
- [33] Y. Diab, F. Ville, P. Velex, Prediction of power losses due to tooth friction in gears, *Tribol. Trans.* 49 (2) (2006) 260–270.
- [34] D. Dowson, G. Higginson, A theory of involute gear lubrication, in: *The Institute of Petroleum, Proceeding of a Symposium on Gear Lubrication-1964*, Elsevier, 1966, pp. 8–15.
- [35] D. Dowson, G.R. Higginson, Reflections on early studies of elasto-hydrodynamic lubrication, in: *IUTAM Symposium on Elastohydrodynamics and Micro-Elastohydrodynamics*, Springer, 2006, pp. 3–21.
- [36] K. Martin, The efficiency of involute spur gears, *ASME J. Mech. Des.* 103 (1) (1981) 160–169.
- [37] V. Simon, Load capacity and efficiency of spur gears in regard to thermo-end lubrication, in: *International Symposium on Gearing and Power Transmissions*, Tokyo, Japan., 1981.
- [38] S. Wu, H. Cheng, A friction model of partial-EHL contacts and its application to power loss in spur gears, *Tribol. Trans.* 34 (3) (1991) 398–407.
- [39] H. Xu, A. Kahraman, N. Anderson, D. Maddock, Prediction of mechanical efficiency of parallel-axis gear pairs, 2007.
- [40] S. Li, A. Vaidyanathan, J. Harianto, A. Kahraman, Influence of design parameters on mechanical power losses of helical gear pairs, *J. Adv. Mech. Des. Syst. Manuf.* 3 (2) (2009) 146–158.
- [41] S. Li, A. Kahraman, A transient mixed elastohydrodynamic lubrication model for spur gear pairs, *J. Tribol.* 132 (1) (2010).
- [42] V.V. Simon, Multi-objective optimization of hypoid gears to improve operating characteristics, *Mech. Mach. Theory* 146 (2020) 103727.
- [43] V.V. Simon, Improvements in the mixed elastohydrodynamic lubrication and in the efficiency of hypoid gears, *Proc. Inst. Mech. Eng. J* 234 (6) (2020) 795–810.
- [44] Z.B. Saribay, Analytical Investigation of the Pericyclic Variable-Speed Transmission System for Helicopter Main-Gearbox (Ph.D. thesis), The Pennsylvania State University, 2009.
- [45] D. Dowson, G.R. Higginson, *Elasto-Hydrodynamic Lubrication*, SI ed., Pergamon Press, New York, 1977.
- [46] H. Xu, A. Kahraman, Prediction of friction-related power losses of hypoid gear pairs, *Proc. Inst. Mech. Eng. K J. Multi-Body Dynam.* 221 (3) (2007) 387–400.
- [47] V.L. Popov, *Contact Mechanics and Friction*, Springer, 2010.
- [48] ISO TC 60, *DTR 13989*.
- [49] C. Cioc, S. Cioc, L. Moraru, A. Kahraman, T.G. Keith Jr., A deterministic elastohydrodynamic lubrication model of high-speed rotorcraft transmission components, *Tribol. Trans.* 45 (4) (2002) 556–562.
- [50] H.R. Hertz, Über die Berührung fester elastischer Körper und über die Härte, in: *Gesammelte Werke*. Bd, Vol. 1, 1882.

- [51] H.A. Zschippang, N. Lanz, K.A. Küçük, S. Weikert, K. Wegener, Face-gear drive: Assessment of load sharing, transmission characteristics and root stress based on a quasi-static analysis, *Mech. Mach. Theory* 151 (2020) 103914.
- [52] Castrol, **Product data sheet: Syntrax universal plus 75W-90**, 2019.
- [53] German Institute for Standardization, Geometrical Product Specifications (GPS)-Surface Texture: profile Method: rules and Procedures for the Assessment of Surface Texture, DIN EN ISO 4288, Beuth Verlag Berlin, Germany, 1996.
- [54] German Institute for Standardization, Geometrical Product Specifications (GPS)-Surface Texture: profile Method-Nominal Characteristics of Contact (Stylus) Instruments, DIN EN ISO 3274, Beuth Verlag Berlin, Germany, 1997.
- [55] SCHAEFFLER, BEARINX-Online easy friction, 2021.
- [56] R. Boness, Churning losses of discs and gears running partially submerged in oil, in: *Proceedings of the ASME International Power Transmission and Gearing Conference*, 1, Chicago, 1989, pp. 355–359.
- [57] C. Changenet, P. Velez, Housing influence on churning losses in geared transmissions, *J. Mech. Des.* 130 (6) (2008).
- [58] C. Changenet, G. Leprince, F. Ville, P. Velez, A note on flow regimes and churning loss modeling, *J. Mech. Des.* 133 (12) (2011).
- [59] British Standard, Gears - Thermal capacity - Part 1: Rating gear drives with thermal equilibrium at 95° C sump temperature, 2001, ISO/TR 14179-1.
- [60] T. Engelke, Einfluss Der Elastomer-Schmierstoff-Kombination Auf Das Betriebsverhalten Von Radialwellendichtringen (Ph.D. thesis), Hannover: Gottfried Wilhelm Leibniz Universität Hannover, 2011.